AAS 17-780

USING SPHERICAL HARMONICS TO MODEL SOLAR RADIATION PRESSURE ACCELERATIONS

Ariadna Farrés[*], Dave Folta[†] and Cassandra Webster[‡]

Solar Radiation Pressure (SRP) is the acceleration produced by the impact of the photons emitted by the Sun on the surface of a satellite. The incident photons are absorbed and reflected by the different components on the satellite's surface, where the rate of absorption and reflection depends on the properties of the satellite's surface material. The acceleration produced by SRP plays an important role on the design and navigation of Libration Point Orbits and interplanetary trajectories. In this paper we introduce an alternative way to obtain high fidelity models for the SRP acceleration using a Spherical Harmonic approximation.

INTRODUCTION

Solar Radiation Pressure (SRP) is the acceleration produced by the impact of the photons emitted by the Sun on the surface of a satellite. The incident light will be absorbed and reflected by the different components on the satellite's surface, where the rate of absorption and reflection will depend on the properties of the surface material. Depending on the orientation of the satellite with respect to the Sun, and the complexity of the satellite's shape and components, this extra acceleration can be hard to determine. Although this extra acceleration exerts a small perturbation on the satellites trajectory, it does play an important role in missions like James Webb Space Telescope (JWST) and Wide-Field Infrared Survey Telescope (WFIRST), due to the sensitivity of the system around Libration Point orbits and on interplanetary missions, like Mars Atmosphere and Volatile EvolutioN Mission (MAVEN) or Rosetta, due to the different satellites' components and large solar panels. An accurate modeling of this effect is important for mission studies in order to reduce the total Δv budget. In this paper we introduce an alternative way to model the SRP acceleration using a Spherical Harmonic approximation.

In literature we find three different ways to model SRP, which we can classify depending on their complexity. The simplest and most common approach is the cannonball model, where the satellite shape is approximated by a sphere. So the SRP acceleration is always along the Sun-satellite direction with a fixed magnitude that depends on the satellite's reflectivity properties. The intermediate approach is known as the N-plate model, where the satellite shape is approximated by N flat plates, each one with different reflectivity properties representing the different satellite's components. One of the advantages of this approach is that the SRP acceleration depends on the satellite's attitude. Nevertheless, it does not take into account possible auto-occultation between the different components of the satellite. Finally, a High-Fidelity model for the SRP was introduced by

[*] Visiting Researcher, NASA Goddard Space Flight Center, Greenbelt, Maryland.
[†] Senior Fellow Chair, NASA Goddard Space Flight Center, Greenbelt, Maryland.
[‡] WFIRST Flight Dynamics Lead, NASA Goddard Space Flight Center, Greenbelt, Maryland.

M. Ziebart,[1,2] which uses ray-tracing techniques to compute all possible impacts of the Sun-light on the surface of the satellite, taking into account its complex shape and reflectivity properties. The main disadvantage of this approach is that it is expensive in terms of computational time and cannot be computed in real time during an orbit simulation. Typically one needs to know the satellite profile in advance, or sample the SRP acceleration for a set of intermediate attitudes and use linear interpolation. Moreover, in order to compute the State Transition Matrix (STM) one has to use linear interpolation for this purpose, which might provide poor estimates of the derivatives.

When considering satellites orbiting around the Earth, the relative Sun-satellite Earth-satellite attitude is repeated over one orbit period, hence SRP is given by a periodic function. As proposed by J. McMahon and D. Scheeres,[3,4] one can use the ray-tracing approach to approximate SRP and a given set of attitudes parameterised θ_{eps} (the Sun-satellite Earth-satellite angle). The Fourier transform can then be applied to approximate this periodic function. Having a trigonometric function approximating SRP acceleration, we can then compute the state transition matrix (STM) and perform perturbation analysis.

In the scenario of a satellite at a Libration Point Orbit (LPO) or on an interplanetary trajectory, the satellite's attitude profile can be more complex and will depend on two angles (λ, θ) related to azimuth and elevation respectively. The natural extension of the Fourier approximation for a function that depends on two angles are the Spherical Harmonics, which we will use to approximate the SRP acceleration. Again, we must sample the SRP function for a fixed set of different attitudes using the ray-tracing techniques[1,2] and approximate this function using Spherical Harmonics (SH). In this paper we will describe how to compute the SH approximation and compare its performance to the N-plate model.

This paper starts with a motivation section where we describe the impact of SRP on Libration point orbits and interplanetary missions. Next we describe the different methods used in literature to derive the SRP acceleration, stating their pros and cons. We also compare their performance on a simple approximation of a GPS satellite using a box-wing approximation. We then introduce the SH approach and how to compute it. Finally we compute the SH approximation of the SRP for the box-wing example and compare it to an N-plate model.

MOTIVATION

Solar Radiation Pressure (SRP) is the acceleration due to the exchange in momenta between the photons emitted by the Sun and the satellite's surface. The force exerted by SRP can be derived from the theories consistent with the fact that light as a particle can push matter. The incident light will be both absorbed and reflected by the surface of the satellite. The rate of absorption and reflection will depend on the properties of the surface material. Hence, the total acceleration due to SRP will vary depending on the shape of the satellite, the materials of the different components, and its relative orientation with respect to the Sun-satellite line. It is true that this extra acceleration is very small compared to the gravitational pull and other perturbations in space.[5] However, for long duration propagation and navigation solutions this effect is relevant and must be take into account.

To illustrate the importance of this effect we want to focus on Wide-Field Infrared Survey Telescope (WFIRST) and Mars Atmosphere and Volatile EvolutioN Mission (MAVEN), two missions with very different objectives and mission scenarios. On one hand, WFIRST is a NASA observatory designed to answer questions about dark energy and astrophysics. It is planned for launch in 2026 to orbit about the Sun-Earth L_2 Libration Point. On the other hand, MAVEN is a space probe de-

veloped by NASA designed to study the Martian atmosphere while orbiting Mars. It was launched in 2013 and on September 2014 was inserted into an elliptic orbit around the red planet.

The estimated area-to-mass ratio for WFIRST is of 0.00675 m^2/kg. One can study how this affects the natural dynamics of the Halo and Quasi-Halo orbits. We know that including the SRP acceleration, assuming a simple cannonball model, will displace the position of SEL2 about 200 km from its classical location in the Restricted Three Body Problem (RTBP). This also happens for the Halo and Quasi-Halo orbits, where the orbits are displaced towards the Sun and their orbital periods also vary. Hence a good modeling of the SRP acceleration can help determine a good nominal orbit and potentially reduce the total Δv budget.

MAVEN on the other hand has an estimated area-to-mass ratio of 0.03118 m^2/kg. If we look at the effect of SRP on a classical Hohmann transfer orbit between Earth and Mars, one can see that there is a difference of about 3000 km on the final position if we compare the simulations including and discarding the SRP acceleration. Again we see the importance of having an accurate modeling of the SRP acceleration during the preliminary design of a mission.

STATE OF THE ART

It is known that the SRP force exerted on an object at a distance R from the Sun is given by:[6]

$$P_{srp} = \frac{P_0}{c}\left(\frac{R_0}{R}\right)^2 = 4.57 \times 10^{-6}\left(\frac{R_0}{R}\right)^2 \ [\text{N/m}^2],$$

where $P_0 = 1367$ W/m^2 is the solar flux at 1 AU, $c = 299792458$ m/s is the speed of light and R_0 is the Sun-Earth distance. Notice that this force is inversely proportional to the distance to the Sun.

If we consider a flat surface, the total force due to SRP is the sum of the acceleration produced by: the photons that are absorbed ($\mathbf{F}_a$) and the photons that are reflected, which experience both: specular reflection ($\mathbf{F}_s$) and diffusive reflection ($\mathbf{F}_d$). The force due to these three effects is given by:

$$\begin{aligned} \mathbf{F}_a &= P_{srp} A \langle \mathbf{n}, \mathbf{r_s} \rangle \mathbf{r_s}, \\ \mathbf{F}_s &= 2 P_{srp} A \langle \mathbf{n}, \mathbf{r_s} \rangle^2 \mathbf{n}, \\ \mathbf{F}_d &= P_{srp} A \langle \mathbf{n}, \mathbf{r_s} \rangle (\mathbf{r_s} + \tfrac{2}{3}\mathbf{n}), \end{aligned} \tag{1}$$

where A is the surface's area, $\mathbf{n}$ denotes the normal vector to the surface, and $\mathbf{r_s}$ is a unitary vector defining the Sun-satellite direction. Figure 1 show a schematic representation of these three different effects on a flat surface.

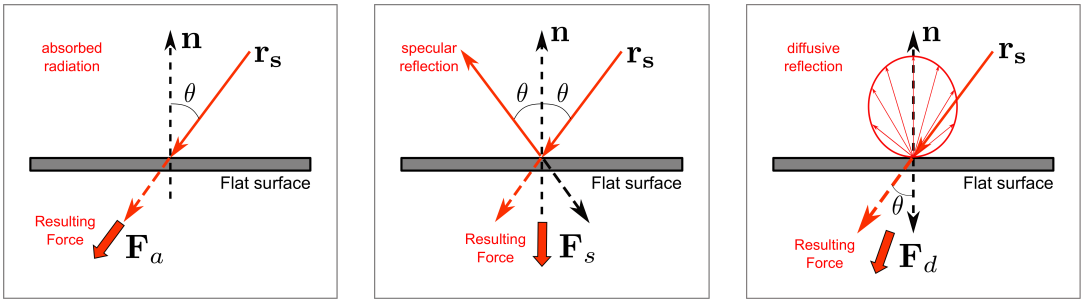

Figure 1. Schematic representation of the force due to absorption, specular reflection and diffusive reflection on a flat surface.

We define the coefficients ρ_a, ρ_s, ρ_d as the rates of absorption, specular and diffusion, which depend on the properties of the surface material, and satisfy $\rho_a + \rho_s + \rho_d = 1$. We use this equality to reduce the number of coefficients, i.e. $\rho_a = 1 - \rho_s - \rho_d$. Hence, the total SRP force exerted on a flat surface of area A is given by:

$$\mathbf{F}_{srp} = P_{srp} A \langle \mathbf{n}, \mathbf{r_s} \rangle \left[(1 - \rho_s)\, \mathbf{r_s} + 2 \left(\rho_s \langle \mathbf{n}, \mathbf{r_s} \rangle + \frac{\rho_d}{3} \right) \mathbf{n} \right]. \tag{2}$$

Finally, if we consider a satellite with a more complex shape, the total acceleration on the satellite due to the SRP force is:[6]

$$\mathbf{a}_{srp} = \frac{P_{srp}}{m_{sat}} \int_{\partial\Omega} \langle \mathbf{n}, \mathbf{r_s} \rangle \left[(1 - \rho_s)\, \mathbf{r_s} + 2 \left(\rho_s \langle \mathbf{n}, \mathbf{r_s} \rangle + \frac{\rho_d}{3} \right) \mathbf{n} \right] d\Omega, \tag{3}$$

where m_{sat} is the mass of the satellite, $\partial\Omega$ is the boundary of the surface defining the satellite's shape, and $d\Omega$ is the element of area. We note that the reflectivity properties ρ_a, ρ_s and ρ_d might vary along the surface $\partial\Omega$. Hence, depending on the complexity of the shape and diversity of materials of the satellite, this integral can be hard to estimate.

In practice one has to make some assumptions and simplifications in order to approximate this function. In the literature we find 3 different approaches: a) *Cannonball model* (simplest) approximates the satellite by a sphere; b) *N-plate model* (intermediate) approximates the satellite by flat plates; c) *Finite Element model* (high-fidelity) approximates the satellite with a CAD model and uses Ray-Tracing techniques to find the illuminated components of the satellite). In the following subsections we will briefly describe these three approaches and as an example to compare the different models we use a a GPS satellite that can be approximated by a simple box-wing model.

Cannonball Model

The cannonball method is the simplest way tot model the SRP acceleration, where we approximate the satellite's shape to be a sphere. It is easy to check that in the case of a sphere, the normal direction to the surface is $\mathbf{n} = -\mathbf{r_s}$, hence $\langle \mathbf{n}, \mathbf{r_s} \rangle = -1$. If we integrate Eq. 3 taking this into account we have that:

$$\mathbf{a}_{srp} = -\frac{P_{srp} C_r A}{m_{sat}} \mathbf{r_s} \ \ [\text{m/s}^2], \tag{4}$$

where A is the projected area and $C_r = (1 + \rho_s + \frac{5}{3}\rho_d)$ is the reflectivity coefficient. Where it is usually assumed that $\rho_d = 0$, so $C_r = (1 + \rho_s)$. The acceleration units are in m/s^2 if the projected area A and the spacecraft mass m_{sat} are given in m and kg respectively.

This model is used in many cases to get an initial understanding of the relevance of the SRP effect on the trajectory of the satellite as it is easy to introduce on the equations of motion. Nowadays, as satellites have larger solar arrays and complex shapes, this approach fails to provide good long term predictions. The N-plate model provides a more accurate representation for satellite's shape.

N-plate Model

The N-plate model approximates the shape of the satellite by a collection of flat plates, each of them having different reflectivity properties. Now the magnitude of the SRP acceleration will vary depending on the satellite's orientation with respect to the Sun.

In this approach, each flat plate is defined by: the normal vector to the surface $\mathbf{n}$, the area of the plate A, and the reflectivity properties of the plate's material (ρ_a, ρ_s, ρ_d). We recall that $\rho_a =$

$1 - \rho_s - \rho_d$ and that we only need to specify two of the three coefficients: (ρ_s, ρ_d). Using Eq. (3) one can derive that the SRP acceleration for a flat plate is:

$$\mathbf{a}_{srp} = \frac{P_{srp}}{m_{sat}} A \langle \mathbf{n}, \mathbf{r_s} \rangle \left[(1 - \rho_s)\, \mathbf{r_s} + 2 \left(\rho_s \langle \mathbf{n}, \mathbf{r_s} \rangle + \frac{\rho_d}{3} \right) \mathbf{n} \right]. \tag{5}$$

Notice that a flat plate only reflects on one side, hence if the light hits the back side of the plate the SRP should not be counted. If we consider the normal vector to the plate ($\mathbf{n}$) to always point out from the reflective face and $\mathbf{r_s}$ to be the Sun-satellite ray, the face is illuminated by the ray if $\langle \mathbf{n}, \mathbf{r_s} \rangle = \cos\theta < 0$.

Hence, if we have N different flat plates, each one defined by its area (A_i), its normal vector ($\mathbf{n}^i$) and reflectivity properties (ρ_s^i, ρ_d^i), the total SRP acceleration is:

$$\mathbf{a}_{srp} = \frac{P_{srp}}{m_{sat}} \sum_{i=1}^{N} \left(A_i \cos\theta_i \left[(1 - \rho_s^i)\mathbf{r_s} + 2 \left(\rho_s^i \cos\theta_i + \frac{\rho_d^i}{3} \right) \mathbf{n}_i \right] H(\theta_i) \right) \quad [\text{m/s}^2], \tag{6}$$

where $\cos\theta_i = \langle \mathbf{n}_i, \mathbf{r_s} \rangle$, and $H(\theta_i)$ is the illumination condition for the i-th plate:

$$H(\theta_i) = \begin{cases} 1 & \text{if} \quad \cos\theta_i < 0, \\ 0 & \text{if} \quad \cos\theta_i \geq 0. \end{cases}$$

Again, the acceleration units are m/s^2 if the plate's area A and the spacecraft mass m_{sat} are given in m and kg respectively.

The main disadvantage of this approach is that it does not take into account possible auto occultation between the different plates. This is because the plates do not have information on their relative position. If there is an auto occultation between two plates, this would need to be introduced by the user by eliminating one of the plates for certain spacecraft attitudes. Also, there is a limit on the feasible number of plates one can use to model the satellite's structure.

Finite Element Model

In order to take into account the auto occultation between the different satellite components Ziebart[1,2] proposed to use ray-tracing techniques to determine which parts of the satellite are illuminated for certain orientations with respect to $\mathbf{r_s}$.

We begin by defining the satellite structure using simple geometric shapes and provide a CAD model. We approximate the different geometric objects by Finite Element (FE) distribution of triangles or polygons (we prefer to use triangles). Secondly, we consider a plane perpendicular to $\mathbf{r_s}$ at a certain distance from the satellite, commonly known as pixel-array, that represents the solar flux. Then we take a grid of points in this pixel-array and from each point we project a ray in the same direction as $\mathbf{r_s}$ and check if it intersects any of the triangles/polygons on the satellite's surface. In this way we determine which parts of the satellite are illuminated. Using a similar approach we can also check the second and third order reflections of the solar rays on the satellite. Finally, if $\{p_{i,j}\}_{i,j\in\Lambda}$ is the set of points on the satellite that have been hit by a ray from the pixel-array, then the total SRP acceleration is:

$$\mathbf{a}_{srp} = \sum_{i,j\in\Lambda} -A_{pix} \left[(1 - \rho_s^{i,j})\mathbf{r_s} + 2 \left(\rho_s^{i,j} \cos\theta_{i,j} + \frac{\rho_d^{i,j}}{3} \right) \mathbf{n}^{i,j} \right] \quad [\text{m/s}^2], \tag{7}$$

where A_{pix} is the size of the pixels on the pixel array, $\cos\theta_{i,j} = \langle \mathbf{r_s}, \mathbf{n}^{i,j} \rangle$ where $\mathbf{n}^{i,j}$ is the normal direction to the surface polygon that has been hit, and $\rho_s^{i,j}$, $\rho_d^{i,j}$ are its reflectivity properties. Again, the acceleration units will be m/s^2 if the CAD model units for the surface are in m and the spacecraft mass m_{sat} is given in kg.

Further details on how to implement this method can be found in the Thesis by Ziebart[7] and Rivers[8] who used the FE to approximate the SRP acceleration. We note that in order to have an accurate approximation for the SRP acceleration we need a large number of points on the pixel-array (i.e. small pixel area). Unfortunately this will make the computational time increase exponentially. Hence, it is not advisable to compute this simultaneously during an orbit simulation with STK or any other orbit simulation software. One must know the attitude profile in advance and compute the SRP acceleration for each one on the profile, or approximate the value from a set of intermediate attitudes.

In the case of satellites orbiting the Earth, the orbital motion is periodic and so are the nominal attitudes, as the solar panels are always facing the Sun with the communications antenna pointed towards the Earth. One can take advantage of the periodicity of the SRP acceleration and use Fourier series to approximate these function. Ziebart used this idea from the GOLNASS satellite,[1] D. Scheeres and J. MacMahon, have worked on these idea for SRP modeling around asteroids[4] and also LEO satellites.[3]

Example

To compare the SRP acceleration obtained using the three different models, let us look at an example of a GPS IIR satellite, which can be approximated by a cube (representing the bus) and two plates (representing the solar panels). Figure 2 shows the CAD model that we used (created with *Blender**). Each solar panel is 2.6×2.6 m^2, and the bus is 2.5 m high, 1.7 m wide and 2.4 m deep. The reflectivity properties for the bus and the solar panels have been taken from Rodriguez-Solano's paper[9] and are summarized in Table 1. We have assumed that all the sides of the bus have the same reflectivity properties, and that the solar panels have the same absorption properties on both sides.

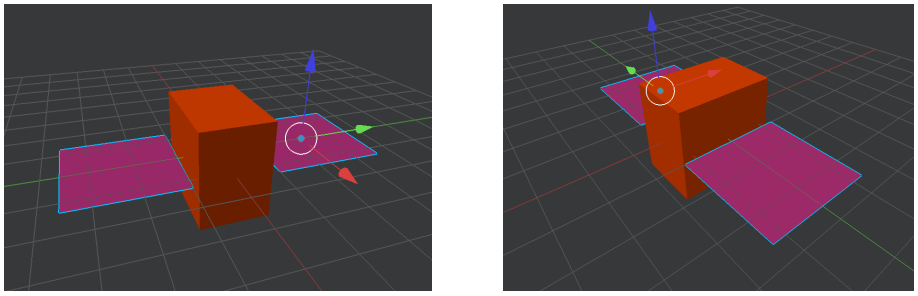

Figure 2. CAD model from Blender of a Box-Wing approximation for a GPS satellite. The color is used to match same reflectivity properties objects.

For the cannonball model approach we consider $A = 17.77$ m^2 as the projected area and $\rho_s = 0.06$ (i.e. $C_r = 1.06$). For the N-plate model we have considered 8 plates (6 for the bus and 2 for the solar panel representing each side), where the area, normal vector and reflectivity properties are derived from Table 1. For the FE model we use the CAD model in Figure 2, where each side of the

*Blender is the free and open source 3D creation suite `https://www.blender.org/`

satellite surface is approximated by two triangles, and the material reflectivity parameters used are the same as in the N-plate model ($\rho_s = 0.06, \rho_d = 0.0$ for the bus and $\rho_s = 0.249, \rho_d = 0.044$ for the two solar panels).

Table 1. For each of the components of a GPS satellite, the normal direction, the reflectivity properties and size area. Data used on the N-plate and Finite Element models to compute the SRP acceleration.

Surface	$\mathbf{n}$	Area (m^2)	ρ_a	ρ_s	ρ_d
2 Solar Panels	$+\mathbf{Z}$, $-\mathbf{Z}$	13.52	0.707	0.249	0.044
Bus (front)	$+\mathbf{X}, -\mathbf{X}$	4.08	0.94	0.06	0.0
Bus (side)	$+\mathbf{Y}, -\mathbf{Y}$	6.00	0.94	0.06	0.0
Bus (top)	$+\mathbf{Z}$, $-\mathbf{Z}$	4.25	0.94	0.06	0.0

For each of the SRP models, we have computed the total SRP acceleration for set of different satellite attitudes. In a body-fixed reference frame we take $\mathbf{r_s} = [-\cos(el)\cos(az), -\cos(el)\sin(az), -\sin(el)]$ as the Sun-satellite direction with $az \in [-180°, 180°]$ and $el \in [-90°, 90°]$ as the azimuth and elevation respectively, taking a set of attitudes $az_i = -180 + i \cdot 10$ and $el_j = -90 + j \cdot 5$ for $i, j = 0, \ldots, 36$.

To have an idea of the computational cost of each method see Table 2, which summarizes the run time of the computation of the SRP acceleration for the 37×37 different attitudes. These computations have been done on a MacBook Pro with a 2,9 GHz Intel Core i5 and that for the FE approach used a mesh of 62500 points on the pixel array, corresponding to a pixel size of 0.0013.

Table 2. Run time for the computation of the SRP for 1369 different attitudes.

	Cannonball	N-plate	Finite Element
Run time	`0.004s`	`0.006s`	`30.518s`

Figure 3 shows the total SRP force $\mathbf{F_{srp}} = (f_x, f_y, f_z)$ for the cannonball model (top), the N-plate model (middle) and the Finite Element model (bottom). As we can see, the cannonball model is a simple approach but in some orientations follows the general trend given by the Finite Element model. Looking at the N-plate and FE results we can see that for certain attitudes the SRP force is slightly different. The main difference is observed on f_y where the auto-occultation by the solar panels have a stronger effect.

We must mention that the force plotted here has been normalized to avoid dealing with small floating point numbers during the computations. The total SRP force at 1 AU has to be scaled by $P_{srp} = 4.57 \times 10^{-6}$. In order to have the total SRP acceleration we must divide the total force by the satellite mass. Assuming that the GPS IIR has a mass of 1100 kg and that we are at 1 AU, all of the plots in Figure 3 have to be multiplied by 4.1453×10^{-9} to have the total SRP acceleration in m/s^2.

Figure 4 compares the total SRP force for each model. The left and middle plots show the total SRP force by the N-plate and FE respectively compared to the cannonball model which is constant. The plot on the far right shows the difference between the N-plate model and the Finite Element model. Note that the total SRP force for the cannonball model is constant, and its magnitude depends on both the area A and its reflectivity coefficient C_r.

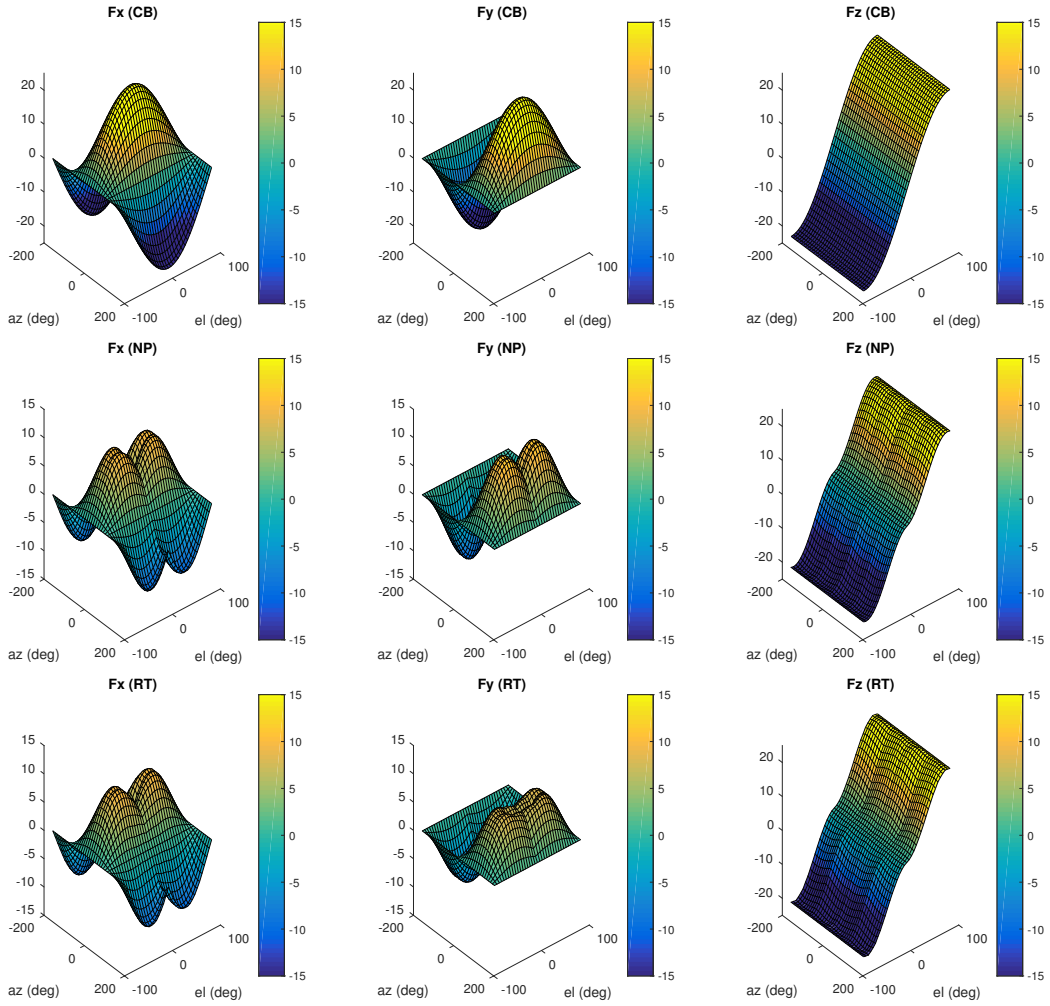

Figure 3. For cannonball (top), N-plate (middle) and Finite Element (bottom) X, Y, Z components of the normalized SRP force $\mathbf{F_{srp}} = (F_X, F_Y, F_Z)$. Multiply by a factor 4.145310^{-9} to have the total acceleration in m/s^2 for a 1100 kg satellite at 1 AU.

In the far right of Figure 4, notice that the maximum difference between the SRP force N-plate and the FE is ≈ 4 in normalized units, which corresponds to a difference of 1.658124×10^{-8} m/s^2 on the total acceleration. Comparing the cannonball approach with both the N-plate and the FE we see that this difference can be up to 15 units, giving and overestimation of 6.217965×10^{-8} m/s^2 for the total SRP acceleration.

SPHERICAL HARMONICS FOR SRP MODELING

The most accurate way to approximate the SRP acceleration is using the Finite Element approach. However, as we have mentioned in the previous section, this approach is computationally very expensive and cannot be done during a real time orbit simulation. This means that we either need to have information of the satellite's attitude along the orbit beforehand, or use function interpolation to recover the SRP acceleration from the one given at intermediate attitudes (az, el).

In the case of a satellite orbiting the Earth, the Sun-Earth-Satellite configuration is fixed, as the

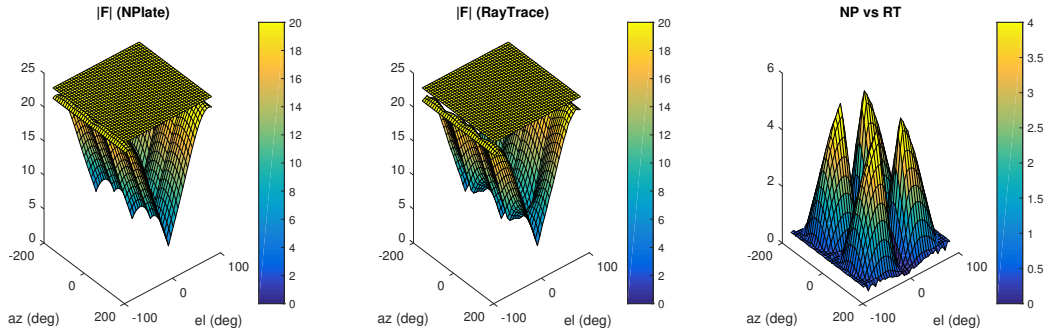

Figure 4. Total SRP normalized force for N-plate and Cannonball (left), Total SRP normalized force for FE and Cannonball (middle), Difference between N-plate and FE SRP force (right). Multiply by a factor $PS = 4.145310^{-9}$ to have the total acceleration in m/s^2 for a 1100 kg satellite at 1 AU.

satellite attitude is set such that the antenna remains pointed towards the Earth and the solar panels are facing the Sun. Since the satellites attitude varies in a periodic way, so will the SRP acceleration. If θ_{EPS} is the angle between the Sun-Earth and Sun-Satellite vectors, one can define the SRP acceleration as a periodic function with respect to θ_{EPS}, and take advantage of the periodicity by using Fourier series to approximate it.

Hence, one can use the FE algorithm to compute the SRP acceleration for a set of different $\theta^k_{EPS} \in [0, 2\pi]$ and compute the Fourier series from the nodes. Although this computation can be difficult depending on the complexity and size of the pixel array, this will only be done once. During the orbit simulations the user only has to evaluate the Fourier series to have the SRP acceleration. The cost of evaluating a Fourier series is negligible and with a few nodes we can recover the SRP acceleration with the desired precision. Moreover, we have the SRP acceleration given by a differential function, which is very useful for perturbation analysis. Ziebart[1] used this idea to improve the orbit determination for GLONASS. Scheeres and McMahon[3,4] have also studied this approach and used it in many different applications.

Nevertheless, when we are looking at LPO like WFIRST or an interplanetary mission like MAVEN, the attitude of the satellite is not periodic and depends on both attitude angles, so we cannot use Fourier series. But what is true, is that the satellite's attitude is defined on a sphere and we can take advantage of this. M.Ziebart[2] suggested to use Spherical Harmonics as it is the natural way to approximate a function defined on the sphere. Looking at the literature we have not seen further references on that, which is why we have decided to explore in this direction.

What are Spherical Harmonics

The Spherical Harmonics (SH) are a set of orthonormal functions defined on the sphere, and can be used to represent functions defined on the surface of a sphere. In the same way as periodic functions (sines and cosines) are used to represent functions defined on a circle via a Fourier series. In mathematics and physical science, they are often employed in solving partial differential equations. In space mechanics they are used when approximating the gravitational potential of planets and asteroids.

The SH are a complete set of orthonormal functions, as they form an orthonormal basis on the Hilbert space of square-integrable functions. This means that on the unit sphere, any square-

integrable function $f(\theta, \lambda)$ can be expanded as a linear combination of these functions:

$$f(\theta, \lambda) = \sum_{n=0}^{\infty} \sum_{m=0}^{n} \left[A_{nm} \cos m\lambda + B_{nm} \sin m\lambda\right] \bar{P}_{nm}(\cos\theta). \tag{8}$$

This expansion holds in the sense of mean-square convergence (convergence in L^2 of the sphere). Hence, if $f_N(\theta, \lambda)$ is the truncated series up to degree N, then $f_N(\theta, \lambda)$ converges to $f(\theta, \lambda)$:

$$\lim_{N\to\infty} \int_0^{2\pi} \int_0^{\pi} |f(\theta, \lambda) - f_N(\theta, \lambda)|^2 \sin\theta \, d\theta \, d\lambda = 0.$$

The coefficients in the expansion (A_{nm}, B_{nm}) are the analogs of Fourier coefficients, and can be obtained by multiplying the above equation by the complex conjugate of a spherical harmonic and integrating over the sphere using the orthogonality relationships. Hence,

$$\left\{ \begin{array}{c} A_{nm} \\ B_{nm} \end{array} \right\} = \frac{1}{4\pi} \int_0^{2\pi} \int_0^{\pi} f(\theta, \lambda) \left\{ \begin{array}{c} \cos(m\lambda) \\ \sin(m\lambda) \end{array} \right\} \bar{P}_{nm}(\cos\theta) \sin\theta \, d\theta \, d\lambda, \tag{9}$$

where $\bar{P}_{nm}(x)$ are the normalized associated Legendre Polynomials.[10]

We will use the SH approximation up to degree N to have an approximation of the SRP acceleration. In order to compute the A_{nm}, B_{nm} one has to approximate the integrals in Eq. 9. There are many ways to compute this in an efficient way.[11] We have computed these coefficients using a double quadrature formula, but there are many approximating formulas that can be used.[12] Next we describe the approach that we have used. For further details on how to derive the following equations see Reference.[13]

Computation of A_{nm}, B_{nm} coefficients

To obtain the coefficients A_{nm}, B_{nm} up to degree N (for $n = 0, \ldots, N$ and $m = 0, \ldots, n$) we need to sample $f(\theta, \lambda)$ on at least $2N \times 2N$ points. Hence, if we take a set of equidistant angles, $\theta_i = i\pi/2N$, $\lambda_j = j\pi/N$ for $i, j = 0, 1, \ldots, 2N-1$, and the images $f(\theta_i, \lambda_j)$, one can see that the integral on Eq. 8 can be approximated by:

$$\left\{ \begin{array}{c} A_{nm} \\ B_{nm} \end{array} \right\} = \frac{\pi}{N} \sum_{i=0}^{2N-1} \sum_{j=0}^{2N-1} d_i f(\theta_i, \lambda_j) \left\{ \begin{array}{c} \cos m\lambda_j \\ \sin m\lambda_j \end{array} \right\} \bar{P}_{nm}(\cos\theta_i), \tag{10}$$

where $d_i = \dfrac{\sqrt{2}}{N} \sin\left(\dfrac{i\pi}{2N}\right) \displaystyle\sum_{h=0}^{N-1} \frac{1}{2h+1} \sin\left((2h+1)\frac{i\pi}{2N}\right)$.

The coefficients A_{nm}, B_{nm} can be easily obtained by evaluating the previous equation in two steps:

$$\begin{array}{ll} A_m(\theta_i) = \displaystyle\sum_{j=0}^{2N-1} f(\theta_i, \lambda_j) \cos m\lambda_j & A_{nm} = \dfrac{\pi}{N} \displaystyle\sum_{i=0}^{2N-1} d_i A_m(\theta_i) \bar{P}_{nm}(\cos\theta_i) \\ & \Rightarrow \\ B_m(\theta_i) = \displaystyle\sum_{j=0}^{2N-1} f(\theta_i, \lambda_j) \sin m\lambda_j & B_{nm} = \dfrac{\pi}{N} \displaystyle\sum_{i=0}^{2N-1} d_i B_m(\theta_i) \bar{P}_{nm}(\cos\theta_i) \end{array}$$

Notice that from the two expression on the left, computing $A_m(\theta_i), B_m(\theta_i)$ is like finding the Fourier coefficients for $f(\theta_i, \lambda)$, and the expression on the left corresponds to the approximation for integrals of $A_m(\theta)P_{nm}(\cos\theta)$ and $B_m(\theta)P_{nm}(\cos\theta)$.

The Legendre polynomials $\bar{P}_{nm}(\cos\theta)$ are evaluated using recurrent formulas that we detail later. As we need their evaluation for different values of θ_i, we will compute them in advance and store them in a table in order to save computational time as they have to be evaluated for each A_{nm}, B_{nm} that we compute.

Evaluation of $f_N(\theta, \lambda)$

Let us now assume that we know the coefficients A_{nm}, B_{nm} for $m = 0, \ldots, N$ and $n = m, \ldots, N$, and what we want is to evaluate the truncated series in Eq. 8. We also do this evaluation in two steps:

$$\left.\begin{aligned} A_m(\theta) &= \sum_{n=m}^{N} A_{nm}\bar{P}_{nm}(\cos\theta) \\ B_m(\theta) &= \sum_{n=m}^{N} B_{nm}\bar{P}_{nm}(\cos\theta) \end{aligned}\right\} \quad \Rightarrow \quad f_N(\theta,\lambda) = \sum_{m=0}^{N} [A_m(\theta)\cos m\lambda + B_m(\theta)\sin m\lambda]$$

The evaluation of $f_N(\theta, \lambda)$ will be used by the orbit simulator, hence it has to be optimized. Notice that the first step requires the evaluation of the Legendre Polynomials, which can be done quickly by using recurrent formulas. The second step is the same as a Fourier evaluation, which can be sped up using Fast Fourier Transforms techniques if required.

Evaluation the Legendre Polynomials

The evaluation of the associated Legendre Polynomials $\bar{P}_{nm}(\cos\theta)$ can optimized if we use the following recurrent expressions.

We start with $\bar{P}_{00}(\cos\theta) = 1, \bar{P}_{10}(\cos\theta) = \sqrt{3}2\cos\theta$.

For $m = 1, \ldots, N$ and $n = m, \ldots, N$:

$$\bar{P}_{nm}(\cos\theta) = M_{nm}\cos\theta\bar{P}_{(n-1)m}(\cos\theta) - N_{nm}\bar{P}_{(n-2)m}(\cos\theta), \tag{11}$$

$$\bar{P}_{nn}(\cos\theta) = \sqrt{\frac{2n+1}{2n}}\sin\theta\bar{P}_{(n-1)(n-1)}(\cos\theta), \tag{12}$$

$$\bar{P}_{(n+1)m}(\cos\theta) = \sqrt{2n+3}\cos\theta\bar{P}_{nm}(\cos\theta), \tag{13}$$

where $M_{nm} = \sqrt{\frac{(2n-1)(2n+1)}{(n-m)(n+m)}}$ and $N_{nm} = \sqrt{\frac{(2n+1)(n+m-1)(n-m-1)}{(2n-3)(n+m)(n-m)}}$.

Notice that this recurrence evaluates the P_{nm} in the same order as we compute the coefficients A_{nm}, B_{nm}. This can be used in order to optimize the evaluation of $f_N(\theta, \lambda)$.

Computing $\mathbf{F}_{srp}(el, az)$ using the Spherical Harmonics

With all of the concepts and formulas explained above we are now ready to use the SH to approximate the SRP acceleration. Let us consider a body-fixed reference frame and use the angles (θ, λ) to define the satellite's attitude with respect to the Sun line. In the SH approximation these two angles are related to the spherical coordinates longitude/zenith (θ) and latitude/azimuth (λ). We can easily translate these two angles to elevation (el) and azimuth (az). Figure 5 shows the relation between both. Using these two angles (θ, λ), the Sun position in the body-fixed reference frame is $\mathbf{x_s} = [\sin\theta\cos\lambda, \sin\theta\sin\lambda, \cos\theta]$ with $\theta \in [0, \pi]$ and $\lambda \in [0, 2\pi]$ (i.e. $\mathbf{r_s} = -\mathbf{x_s}$ is the Sun-satellite direction).

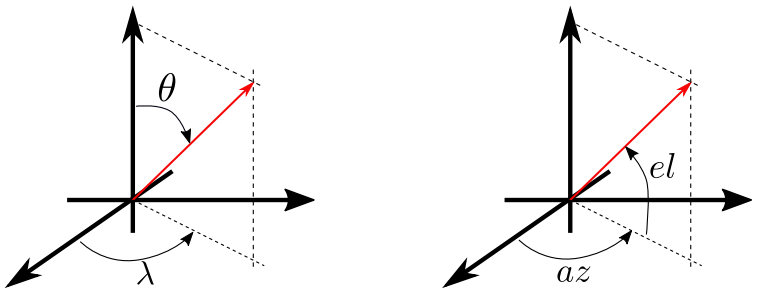

Figure 5. In a body-fixed reference frame. Left: Definition of the longitude (θ) and latitude (λ) angles; Right: Definition of the elevation (el) and azimuth (az) angles.

We start by sampling the function $f_{i,j} = \mathbf{F}_{srp}(\theta_i, \lambda_j)$ in a $2N \times 2N$ equidistant grid of angles: $\theta_i = i\pi/2N$, $\lambda_j = j\pi/N$ for $i, j = 0, 1, \ldots, 2N-1$. We use the FE algorithm to compute each of the $f_{i,j}$ values. Although this process can be computationally expensive, it has to be done only once.

Then we compute the spherical harmonic coefficients A_{nm}, B_{nm} for $n = 0, \ldots, N$, $m = 0, \ldots, n$ using the two step evaluation described above. Again, this step has to be done only once, so the computational cost is not a critical issue. Note that we compute 3 set of coefficients $A_{nm}^{x,y,z}, B_{nm}^{x,y,z}$, one for each component of $\mathbf{F}_{srp} = (f_x, f_y, f_z)$.

We now have that $\mathbf{F}_{srp}^N = (f_x^N, f_y^N, f_z^N)$, where

$$f_{x,y,z}^N(\theta, \lambda) = \sum_{m=0}^{N} \sum_{n=m}^{N} [A_{nm}^{x,y,z} \cos m\lambda + B_{nm}^{x,y,z} \sin m\lambda] \, \bar{P}_{nm}(\cos\theta). \tag{14}$$

is the approximated SRP force.

During an orbit simulation we use $\mathbf{F}_{srp}^N / m_{sat}$ to approximate SRP acceleration. Note that here we need to evaluate 3 times a SH series of order N for each time step. Hence, the computational time is crucial and needs to be reduced as much as possible. For this reason we must use the Legendre Polynomials recurrences to optimize the process.

Example

To test the performance of the SH approach, we have taken the box-wing CAD model approximation that we described in the introduction section, and used the algorithm described above to find the SH series that approximates the SRP force up to degree 4, 8 and 16. Table 6 (in the Appendix)

shows the coefficients for the SH series for f_x, f_y and f_z up to degree 3. Notice that most of the elements on the series are zero. Once we have computed the SH approximation up to degree 4, 8 and 16, we have evaluated the SH series for grid of different attitudes in order to compare the approximation we have obtained. As we did in Section 2, we have taken a grid of 37×37 different attitudes, $\theta_i = i \cdot 5$, $\lambda_j = -180 + j \cdot 10$ for $i, j = 0, \ldots 36$. In Table 3 (top) we summarize the total run time of evaluating the SH series over the 1369 different attitudes. This table also contains for each of the SH models the maximum error of approximation, considering as true value for the SRP the computed using Finite Elements. As we can see, the computational time increases with the degree of the SH series, but for degree 4 and 8 the cost is comparable to using the N-plate mode. We recall that all the computations have been done on a MacBook Pro with a 2,9 GHz Intel Core i5. As expected, the maximal error using the SH decreases as the degree increases. Moreover, the maximum error for the SH of degree 4 is almost half the maximum error using the N-plate model.

Table 3. For different SH degrees and the N-plate model. Top: run time for the computation of 1369 different attitudes. Bottom: maximum error of approximation.

	FE	N-Plate	SH deg 4	SH deg 8	SH deg 16
Run Time	0m34.226s	0m 0.005s	0m 0.006s	0m 0.008s	0m 0.012s
Max Error	–	4.8426	2.0783	0.8889	0.5457

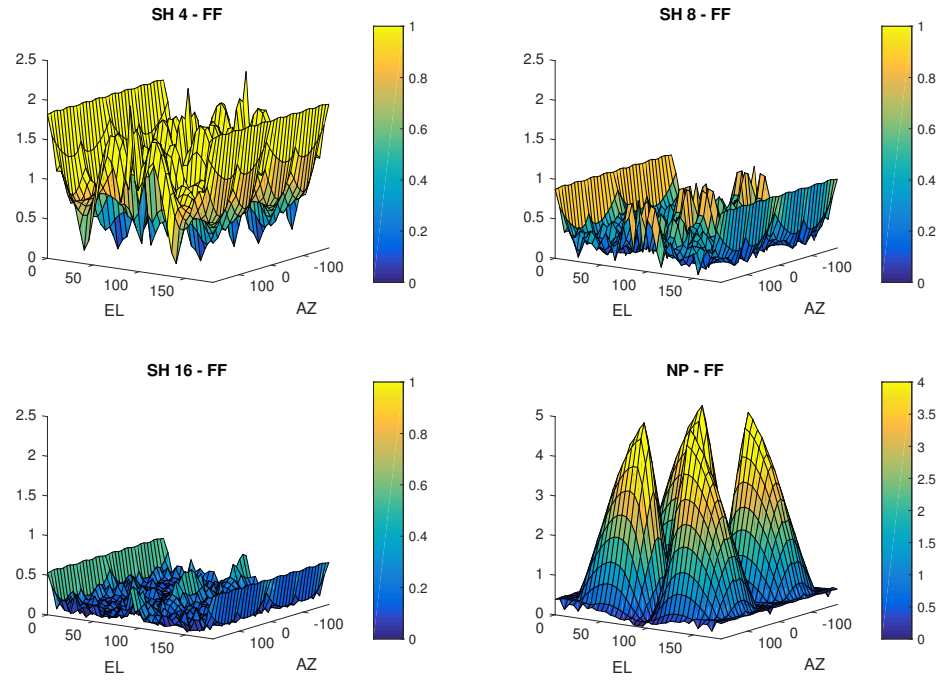

Figure 6. Difference between different SRP force approximations and the FE solution. From left to right, top to bottom difference between the SH approximation for degree 4, degree 8, degree 16 and the N-plate model. Multiply by a factor $PS = 4.145310^{-9}$ to have the total acceleration in m/s^2 for a 1100 kg satellite at 1 AU.

Figure 6 shows for different attitudes, the difference between the different SRP force approximations and the SRP force found using the FE. Plotting the results for the SH up to degree 4, 8 and 16 and the N-plate model. As we can see, as we increase the degree of the SH the error decreases. In

the bottom right plot we have the difference between the SRP using the N-plate model and the FE approach. As we can see this error is larger than the one provided by the SH approximation. These results are very promising as they show the great potential that the SH approximation has.

COMPARISON FOR COMPLEX SATELLITES

In this final section we want to compare the performance of the SH approach with the N-plate model for MAVEN and WFIRST. For both satellites we have approximated the satellites shape by an N-plate model and a 3D CAD model. The CAD model has been designed using Blender, and their representation can be seen in Figure 7. In both approximations (FE vs N-plate) we have considered the same reflectivity properties for the different components. For instance, the bus and telescope are assumed to be recovered with Mylar and have $\rho_s = 0.1, rho_d = 0.42$. In the case of the solar panels, we have chosen different reflectivity properties for both satellites. For WFIRST we have that $\rho_s = 0.037$ and $\rho_d = 0.0414$, and for MAVEN the $+Z$ components of the solar panel have $\rho_s = 0.037$ and $\rho_d = 0.0414$, while the $-Z$ components have $\rho_s = 0.02$ and $\rho_d = 0.23$. We note that the reflectivity properties that we have used are close realistic values, and are chosen to be consistent between the N-plate model and the FE approximation.

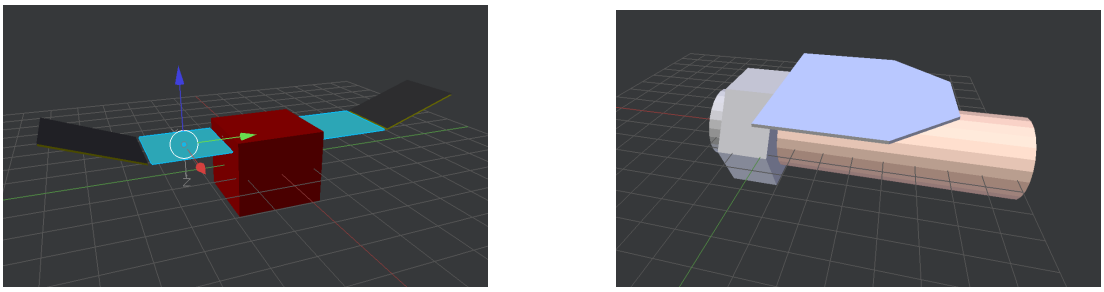

Figure 7. 3D CAD model from Blender for MAVEN (left) and WFIRST (right). The color on each of the components is used to relate objects with the same reflectivity properties.

For each satellite we have computed the SRP force using the different approaches for a set of 37×37 equidistant attitudes $\theta_i = i \cdot 5$, $\lambda_j = -180 + j \cdot 10$ for $i, j = 0, \dots 36$. As before we compare the computational time and the approximation error with the FE approximation using ray-tracing which is considered to be the true SRP force. We recall that all the computations have been done on a MacBook Pro with a 2,9 GHz Intel Core i5.

Comparison for MAVEN

In the case of MAVEN we have used 14 plates to define the N-plate model, 8 plates for the solar panels as we consider different reflectivity properties for one side and the other and 6 plates to define the different Bus sides. In Table 4 (top) we have the computational time for the evaluation of 1369 different attitudes using the FE, the N-Plate and the SH of degrees 4, 8 and 16. Notice that the evaluation of SH up to degree 4 and 8 are of the same order as the N-plate model, while the FE cost is more than 2 min. In the same table (bottom) we have the maximum error of approximation considering the FE SRP approximation as true. Here the maximum error for the SRP force decreases as we increase the SH degree. Moreover, for SH of degree 4 the maximum error is half the maximum error for the N-plate model.

Table 4. For MAVEN, different SH degrees and the N-plate model. Top: run time for the computation of 1369 different attitudes. Bottom: maximum error of approximation.

	FE	N-Plate	SH deg 4	SH deg 8	SH deg 16
Run Time	2m 22.297s	0m 0.007s	0m 0.006s	0m 0.009s	0m 0.014s
Max Error	–	9.0995	4.1791	2.1514	2.0483

In Figure 8 we show for the different attitudes ($az \in [-180°, 180°]$ and $el \in [-90°, 90°]$) the difference between the SRP force approximations and the SRP force found using the FE (i.e. approximation error). We can see how the error decreases uniformly as the degree of the SH increases. We note that the maximum error of the approximation is located close to $el = 90°$. We can also see how in almost all the domain the SH approximation has a smaller error than the N-plate model, mainly due to the auto occultation that are not taken into account on the N-plate model.

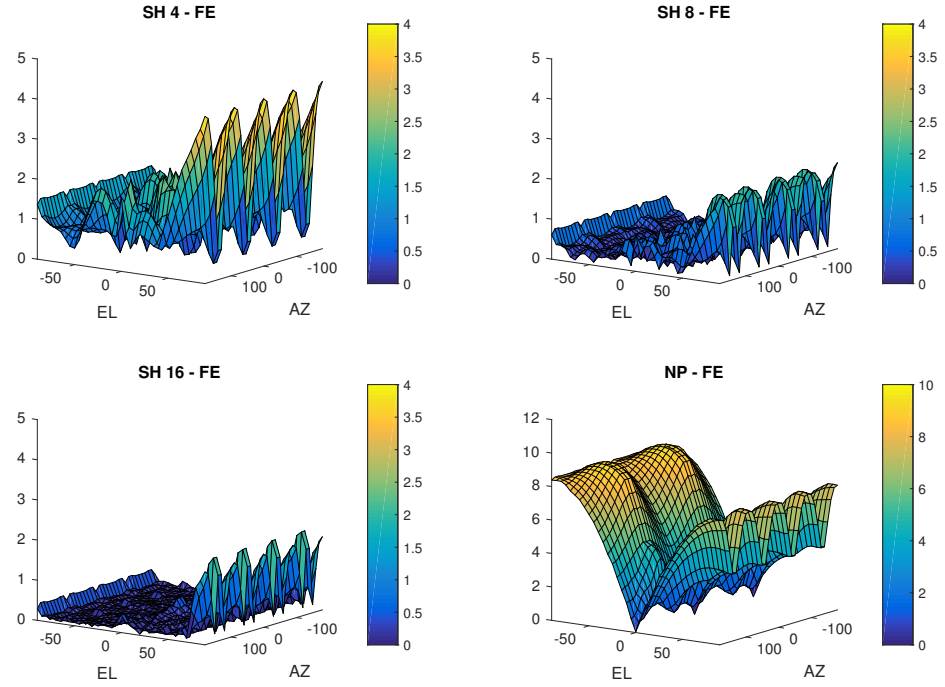

Figure 8. For MAVEN, difference between different SRP force approximations and the FE solution. From left to right, top to bottom difference between the SH approximation for degree 4, degree 8, degree 16 and the N-plate model. Multiply by a factor $PS = 5.636410^{-9}$ to have the total acceleration in m/s^2 considering a dry mass of 809 kg and the satellite at 1 AU from the Sun.

Comparison for WFIRST

As we can see in Figure 7 WFIRST has a more complex shape. It is composed by a flat solar panel, a cylinder that approximating the telescope shape, and an hexagon for the bus, where the thruster and other components of the satellite are placed. To design the N-plate model we have considered 14 different plates: 2 plates to define the solar panel, 6 plates to approximate the cylinder as a rectangular cube, 6 more plates to approximate each of the hexagon faces. Again we have evaluated the 1369 different attitudes using the FE, the N-Plate and the SH of f degrees 4, 8 and

16, and the results are summarized in Table 5. Notice how the computational time using the FE approximation has increased, compared to MAVEN and the GPS IIR satellites (Table 4 and **??** respectively). This is due to the fact that the CAD model for WFIRST is composed by more Finite Elements than the other two satellites due to its complexity.

In Table 5 we observe the same behavior as before, the maximum error decreases as we increase the degree of the SH and this one is always less than the error for the N-plate approximation. Moreover, the computational time using the N-plate model and the SH of degree 4 are comparable.

Table 5. For WFIRST, different SH degrees and the N-plate model. Top: run time for the computation of 1369 different attitudes. Bottom: maximum error of approximation.

	FE	N-Plate	SH deg 4	SH deg 8	SH deg 16
Run Time	19m 48.242s	0m 0.007s	0m 0.007s	0m 0.009s	0m 0.013s
Max Error	–	10.0703	5.2488	2.6050	1.3086

Finally, in Figure 9 we show the for different attitudes ($az \in [-180°, 180°]$ and $el \in [-90°, 90°]$) the difference between the SRP force approximations and the SRP force found using the FE (i.e. approximation error). Again the error decreases uniformly as we increase the SH degree, and for all the degrees the SH give a better approximation than the N-plate model.

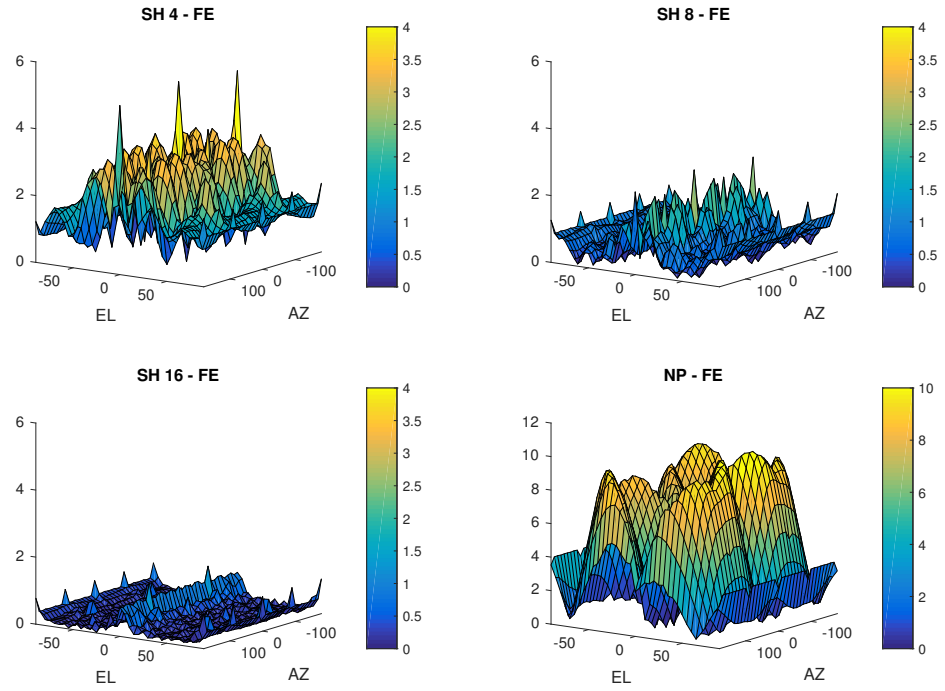

Figure 9. For WFIRST difference between different SRP force approximations and the FE solution. From left to right, top to bottom difference between the SH approximation for degree 4, degree 8, degree 16 and the N-plate model. Multiply by a factor $PS = 6.2055610^{-10}$ to have the total acceleration in m/s^2 considering a dry mass of 7348 kg and the satellite at 1 AU from the Sun.

CONCLUSION & FUTURE WORK

In this paper we present an alternative way to produce High-Fidelity models for SRP by using Spherical Harmonics (SH). Classically, in order to have a High-Fidelity model for SRP one must use Finite Elements (FE) to approximate the satellites structure, and ray-tracing tools to find the illuminated area and derive the total SRP acceleration. The main drawback of this approach is the computational cost. We have seen that we can considerably reduce this cost by interpolating the SRP acceleration provided by the FE with SH. The SH provide a high accuracy approximation of the SRP acceleration with a small amount of sample points. Moreover, we are approximating the SRP by a differential function which enables us to do perturbation theory analysis.

We have computed the SH approximation for the SRP acceleration of different example satellites (i.e. GPS IIR, MAVEN and WFIRST) and compared the SH with the N-plate model. We have seen that the computational cost of evaluating the SH series up to degree 4 is comparable to the computational cost of evaluating the N-plate model. Moreover the SH give a higher accuracy approximation of the total SRP acceleration than the N-plate model.

We must mention that the algorithms that we have produced can still be improved in many directions and we are currently working on them. For instance, in terms of the computational cost, as we can see in Table 6 most of the coefficients in the SH are zero, this can be taken into account and reduce the evaluation cost. On the other hand, looking at the errors given by the SH approach (Figure 6), one notices that the error approximation is higher on the poles, i.e. for elevations close to $\pm 90^\circ$ ($\pm\mathbf{Z}$). This is common when approximating functions on the sphere, and in some cases can be solved by changing the sampling set. We recall that we have taken a grid of attitudes uniformly distributed in $\theta \in [0, \pi]$ and $\lambda \in [0, 2\pi]$, having a larger concentration of points on the Poles than on the equator. One could use a uniform distribution of points on the sphere to compute the SH coefficients A_{nm}, B_{nm} expecting a better behavior near the Poles. We note that changing the sampling set of attitudes can change the quadrature formulas used to find the SH coefficients.

APPENDIX: SH COEFFICIENTS

Table 6. For GPS IIR: the Spherical Harmonics coefficients up to degree 3 to approximate f_x, f_y, f_z.

nm	A^x_{nm}	B^x_{nm}	A^y_{nm}	B^y_{nm}	A^z_{nm}	B^z_{nm}
00	2.7855e-17	0.0000e+00	-1.1674e-17	0.0000e+00	5.8309e-14	0.0000e+00
10	1.1847e-18	0.0000e+00	-2.1432e-17	0.0000e+00	1.0187e+01	0.0000e+00
11	5.7466e+00	-9.4506e-16	-1.0537e-15	5.4313e+00	-1.8686e-18	9.1266e-17
20	1.2795e-17	0.0000e+00	2.7602e-17	0.0000e+00	1.6878e-15	0.0000e+00
21	2.8405e-15	2.0419e-16	8.2080e-17	-1.3756e-15	-4.9789e-16	-1.1269e-16
22	-8.1257e-16	-4.2933e-16	-1.7994e-16	-2.3232e-16	-4.7421e-14	-2.4590e-16
30	-9.3624e-18	0.0000e+00	-8.6312e-18	0.0000e+00	1.9505e+00	0.0000e+00
31	1.3601e+00	-2.1735e-16	-1.3972e-15	1.1530e+00	-1.0545e-17	1.4967e-16
32	-7.5663e-17	3.7823e-17	1.3203e-17	1.1033e-17	4.4185e-01	4.8805e-16
33	-3.8333e-02	-9.5323e-16	-6.0268e-16	3.2223e-01	-8.6937e-18	6.9630e-17

Table 7. For MAVEN: the Spherical Harmonics coefficients up to degree 3 to approximate f_x, f_y, f_z.

nm	A^x_{nm}	B^x_{nm}	A^y_{nm}	B^y_{nm}	A^z_{nm}	B^z_{nm}
00	-2.0897e-16	0.0000e+00	1.9395e-17	0.0000e+00	8.1419e-01	0.0000e+00
10	-1.1288e-17	0.0000e+00	5.0201e-18	0.0000e+00	7.4999e+00	0.0000e+00
11	5.5927e+00	-1.7320e-15	2.7297e-16	5.5912e+00	-3.0503e-17	9.9981e-18
20	1.7086e-17	0.0000e+00	3.6743e-17	0.0000e+00	5.4580e-01	0.0000e+00
21	3.2306e-01	9.0049e-16	8.2037e-17	7.4909e-01	-3.4642e-16	-7.3896e-17
22	-2.8295e-16	3.2135e-16	1.6250e-16	-2.4355e-16	-1.4846e-01	-4.6969e-17
30	-4.5637e-18	0.0000e+00	9.9410e-17	0.0000e+00	1.1771e+00	0.0000e+00
31	1.4324e+00	5.4801e-16	-1.4385e-16	1.3320e+00	-3.5717e-17	2.8442e-17
32	-5.3561e-17	6.0070e-17	4.9185e-17	3.4240e-18	1.1400e-01	1.3740e-17
33	-4.9053e-01	-1.3918e-15	3.4936e-16	5.4616e-01	-5.0166e-17	-7.0004e-17

Table 8. For WFIRST: the Spherical Harmonics coefficients up to degree 3 to approximate f_x, f_y, f_z.

nm	A^x_{nm}	B^x_{nm}	A^y_{nm}	B^y_{nm}	A^z_{nm}	B^z_{nm}
00	4.5310e-02	0.0000e+00	1.0164e-15	0.0000e+00	1.5868e+00	0.0000e+00
10	-2.0077e-01	0.0000e+00	5.6821e-16	0.0000e+00	2.1866e+01	0.0000e+00
11	1.5972e+01	-1.9312e-15	-1.8167e-15	1.8304e+01	-2.3081e-01	6.1291e-16
20	1.0438e-02	0.0000e+00	-1.3277e-15	0.0000e+00	9.3322e-01	0.0000e+00
21	3.3917e-01	-4.2446e-15	-1.1873e-15	4.3208e-01	-7.0827e-02	9.4158e-16
22	3.6778e-02	3.8795e-16	-6.2276e-16	-3.1597e-03	-5.4566e-03	-8.9949e-16
30	1.7954e-01	0.0000e+00	1.2411e-15	0.0000e+00	3.1088e+00	0.0000e+00
31	3.8480e+00	-1.7260e-15	-4.9471e-16	2.6299e+00	-2.3070e-01	3.3836e-15
32	-2.6930e-01	3.2906e-16	-6.9876e-16	-1.6290e-01	-1.1166e+00	1.1444e-15
33	-2.6372e+00	-6.3294e-16	2.5294e-15	-9.6609e-01	-4.1356e-02	1.0390e-15

ACKNOWLEDGMENT

The work has been funded under the Goddard Planetary Heliophysics Institute Task 595.001 in collaboration with the University of Maryland Baltimore County (UMBC) under the NNG11PL02A. The attendance to the conference has been supported by the Spanish grant MTM2015-67724-P (MINECO/FEDER) and the Catalan grant 2014 SGR 1145.

REFERENCES

[1] M. Ziebart and P. Dare, "Analytical Solar Radiation Pressure Modelling for GLONASS using a pixel array," *Journal of Geodesy*, Vol. 75, 2001, pp. 587–599, 10.1007/s001900000136.

[2] M. Ziebart, "Generalized Analytical Solar Radiation Pressure Modeling Algorithm for Spacecraft of Complex Shape," *Journal of Spacecraft and Rockets*, Vol. 41, No. 5, 2004.

[3] J. W. McMahon and D. J. Scheeres, "New Solar Radiation Pressure Force Model for Navigation," *Journal of Guidance, Control and Dynamicsi*, Vol. 33, 2010, pp. 1418–1429, 10.2514/1.48434.

[4] S. G. Hesar, D. J. Scheeres, and J. W. McMahon, "Precise Solar Radiation Pressure Models for Small-Body Orbiters: Applications to OSIRIS-REx Spacecraft," *Journal of Guidance, Control, and Dynamics*, Vol. 40, No. 7, 2017, pp. 1638–1650, 10.2514/1.G002323.

[5] R. P. Russell, "Survery of Spacecraft Trajectory Desing in Stronfly Perturbed Enviroments," *Journal of Guidance, Control, and Dynamics*, Vol. 35, No. 3, 2012, pp. 705–720, 10.2514/1.56813.

[6] A. Milani, A. Nobill, and P. Farinella, *Non-gravitational perturbations and satellite geodesy*. Adam Hilger Ltd.,Accord, MA, 1987.

[7] M. Ziebart, *High precision analytical solar radiation pressure modelling for GNSS spacecraft*. PhD thesis, University of East London, 2001.

[8] B. Rievers, *High precision modelling of thermal perturbations with application to Pioneer 10 and Rosetta*. PhD thesis, University of Bremen, 2012.

[9] C. Rodriguez-Solano, U. Hugentobler, and P. Steigenberger, "Adjustable box-wing model for solar radiation pressure impacting GPS satellites," *Advances in Space Research*, Vol. 49, No. 7, 2012, pp. 1113–1128, 10.1016/j.asr.2012.01.016.

[10] M. Abramowitz, *Handbook of Mathematical Functions, With Formulas, Graphs, and Mathematical Tables,*. Dover Publications, Incorporated, 1974.

[11] N. Sneeuw, "Global spherical Harmoncs analysis by least-squares and numerical quadrature methods in historical prespective," *Geophysical Journal Intermational*, Vol. 118, 1994, pp. 707–716.

[12] I. H. Sloan and R. S. Womersley, "Constructive Polynomial Approximation on the Sphere," *Journal of Approximation Theory*, Vol. 103, No. 1, 2000, pp. 91 – 118, http://dx.doi.org/10.1006/jath.1999.3426.

[13] J. A. R. Blais, D. A. Provins, and M. A. Soofi, "Spherical Harmonics transforms for discrete multiresolution applications," *The Journal of Supercomputing*, Vol. 38, 2006, pp. 173–187.